

Energy-energy correlators in jets across collision systems and parton flavors

Anjali Nambrath^{1,*} on behalf of the ALICE collaboration

¹University of California, Berkeley

Abstract. The two-point energy-energy correlator (EEC) is a novel jet substructure observable probing the correlation of energy flow within jets. In these proceedings, three EEC measurements performed by the ALICE Collaboration are reported. First is a finalized measurement in proton-proton collisions, where the angular dependence of the EEC cross-section shows a separation of the perturbative and non-perturbative regimes. The first EEC measurement is reported in heavy-flavor jets, tagged via a fully-reconstructed D^0 meson. Here, comparison to inclusive pp jets provides insights into the flavor dynamics of QCD fragmentation and hadronization. Finally, the first measurement of EECs in p-Pb collisions is presented. By comparing the results to pp, modifications in jet evolution caused by the presence of a cold nuclear medium can be studied.

1 Introduction

In these proceedings, three measurements performed by the ALICE Collaboration of a novel jet substructure observable called the energy-energy correlator (EEC) [1–3] are presented. The EEC captures the correlation function of energy flow inside jets. It is experimentally defined as an energy-weighted two-particle correlation between pairs of particles inside a jet, as a function of the angular distance (R_L) separating the pair. The energy-energy correlation function, $\Sigma_{\text{EEC}}(R_L)$, is defined as follows:

$$\Sigma_{\text{EEC}}(R_L) = \frac{1}{N_{\text{jet}} \cdot \Delta} \int_{R_L - \frac{1}{2}\Delta}^{R_L + \frac{1}{2}\Delta} \sum_{\text{jets}} \sum_{i,j} \frac{p_{T,i} p_{T,j}}{(p_T^{\text{ch jet}})^2} \delta(R'_L - R_{L,ij}) dR'_L. \quad (1)$$

Here, $p_T^{\text{ch jet}}$ refers to the total charged-particle jet p_T . The sum runs over all particle pairs (i, j) inside the jet. For each pair, an energy weight is calculated: $p_{T,i} p_{T,j} / (p_T^{\text{ch jet}})^2$. The weighted number of track pairs is counted as a function of the angular distance between both tracks, $R_{L,ij} = \sqrt{(\varphi_j - \varphi_i)^2 + (\eta_j - \eta_i)^2}$, where φ and η are the azimuthal angle and pseudorapidity respectively. The angular bin width is Δ , and the EEC is normalized by the total number of jets N_{jet} .

The EEC distribution is characterized by a clear transition region. This is sensitive to the transition between the perturbative and non-perturbative regimes of jet evolution. As jets are angularly ordered objects, with earlier splittings being wider than subsequent ones, the angular scale of the EEC is sensitive to the time evolution of jet formation and allows the eventual confinement of partonic jet constituents to be probed.

*e-mail: nambrath@berkeley.edu

2 Final measurement of EECs in pp collisions

First, the finalized ALICE measurement of EECs in pp collisions is presented [4]. Figure 1 shows the pp EECs in three $p_T^{\text{ch,jet}}$ ranges. A clear $p_T^{\text{ch,jet}}$ dependence in the EEC peak position is observed, with the distribution shifting to smaller angles as $p_T^{\text{ch,jet}}$ increases. Figure 2 shows a universal shape that emerges when we the EEC x -axis is rescaled from R_L to $\langle p_T^{\text{ch,jet}} \rangle R_L$, which is analogous to virtuality. The $p_T^{\text{ch,jet}}$ dependence disappears, and the EEC distributions collapse onto one curve with a clear peak position around 2.4 GeV/c. Figure 2 also shows a comparison to a pQCD calculation [2] – good agreement is observed at very large R_L , suggesting that this region of the EEC maps onto perturbative physics. Similarly, at very small R_L , good agreement with the linear scaling for free hadrons is observed. Together this suggests that the EEC allows a separation of the perturbative and non-perturbative regions. It is worth noting that neither the pQCD calculation nor the linear scaling describe the EEC near the peak, suggesting that the transition between these regions is not sharp.

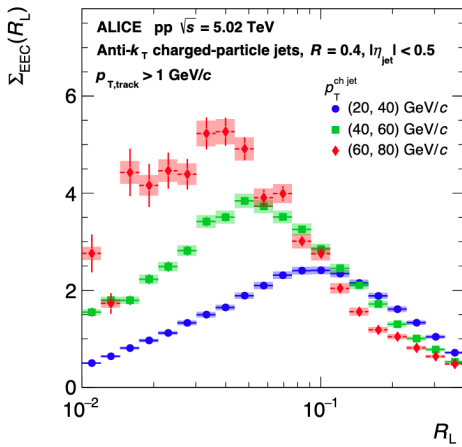


Figure 1. EEC in pp collisions in three $p_T^{\text{ch,jet}}$ ranges: 20–40, 40–60, and 60–80 GeV/c [4]. A clear $p_T^{\text{ch,jet}}$ dependence is seen in the EEC peak, with the distribution shifting to smaller angles as $p_T^{\text{ch,jet}}$ increases.

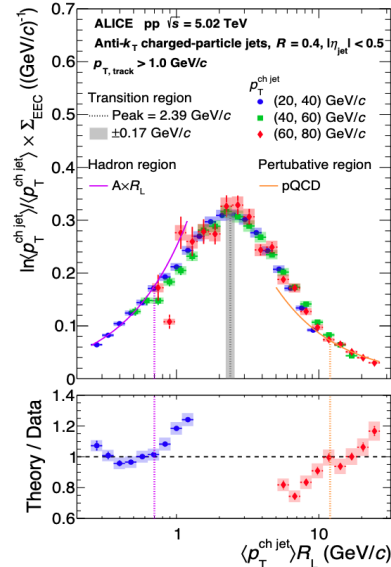


Figure 2. EEC rescaled as a function of $\langle p_T^{\text{ch,jet}} \rangle R_L$, showing the universality of the EEC transition region [4].

3 First measurement of EECs in D^0 -tagged jets in pp collisions

Having established a baseline measurement in inclusive pp jets, EECs in heavy-flavor jets can now be studied. This has been studied in some depth theoretically [5]. Figure 1 in Ref. [5] shows a comparison between EECs in light-quark jets, charm jets, and beauty jets in PYTHIA. A clear mass dependence is observed; the charm and beauty EECs show strong suppression at small angles (a signature of the dead cone). The EEC offers a unique opportunity to probe the dead cone, as its amplitude quantifies the amount of radiation in a jet.

The ALICE measurement of D^0 -tagged jets is shown in Fig. 3. The measurement covers two $p_T^{\text{ch,jet}}$ ranges, 10–15 GeV/c and 15–30 GeV/c. Each jet is required to contain a D^0 meson with $p_T > 5$ GeV/c. The upper panel compares the D^0 -tagged jet EEC to inclusive and semi-inclusive EECs. The semi-inclusive distribution applies a p_T selection on the leading track to study the fragmentation bias introduced by the D^0 p_T selection.

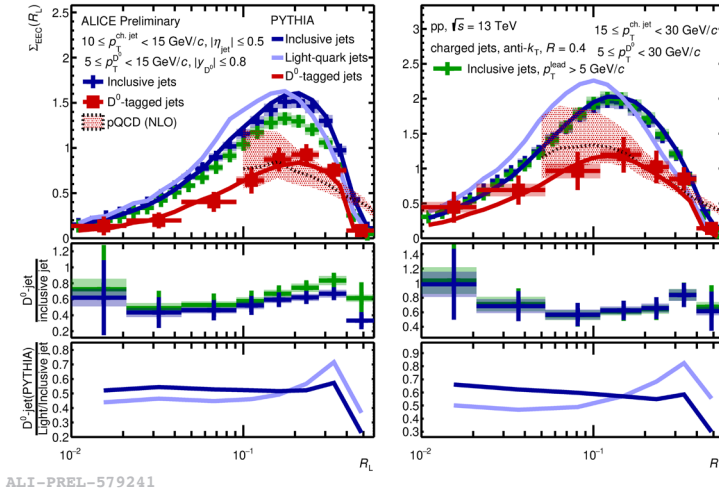


Figure 3. Measurement of EECs in D^0 -tagged jets in pp collisions at $\sqrt{s} = 13$ TeV. The left panel shows results for 10–15 GeV/c jets, and the right panels shows 15–30 GeV/c jets. The D^0 -tagged jet EEC (red) is compared to inclusive jets (blue), PYTHIA (solid lines), and a pQCD calculation (shaded region).

A visible suppression of the D^0 -tagged EEC curves is observed relative to the inclusive EEC over the entire R_L range. These observations are consistent with the expected suppression of radiation from massive quarks due to the dead-cone effect. The selection bias from the minimum D^0 p_T requirement appears to be negligible, based on comparisons of inclusive jets with and without a $p_T^{\text{leading}} > 5$ GeV/c selection. The peak positions of the charm-tagged and inclusive jet EECs are similar in these $p_T^{\text{ch,jet}}$ ranges, and PYTHIA reproduces this. This similarity occurs because inclusive jets are predominantly gluon-initiated, and Casimir effects counterbalance the dead-cone in terms of peak position. In contrast, the measured peak shows tension with the next-to-leading-order (NLO) pQCD calculation [5], suggesting the impact of non-perturbative effects on the charm-quark shower and hadronization processes.

4 Comparison of pp EECs to event generator predictions

Because the EEC has perturbative and non-perturbative regions, it is not unreasonable to associate the transition region with hadronization. This motivates comparisons of these measurements to models with different hadronization mechanisms. Four event generators are considered: PYTHIA 8 [6], Herwig 7 [7], and Sherpa 2.2.15 with two different tunes (Lund and AHADIC) [8]. PYTHIA and Sherpa Lund both use Lund string models, and Herwig and Sherpa AHADIC use cluster models.

Figure 4 in Ref. [4] shows a comparison of the inclusive pp EEC measurement to these generators. The overall shape and amplitude of the EEC are sensitive to the hadronization mechanism, both at small and large R_L . However, the inclusive measurement does not clearly favor any particular hadronization model at the current level of precision [4]. Figure 4 shows the same comparison for D^0 -tagged jets, where PYTHIA is slightly favored. Herwig overpredicts the yield for inclusive jet EECs, but underpredicts heavy-flavor EECs. Sherpa Lund underpredicts the data everywhere, and AHADIC fails to describe the peak entirely. No definitive conclusions can be drawn from these comparisons. The inclusive measurements might suggest that cluster hadronization works better for higher p_T jets, and the D^0 -tagged

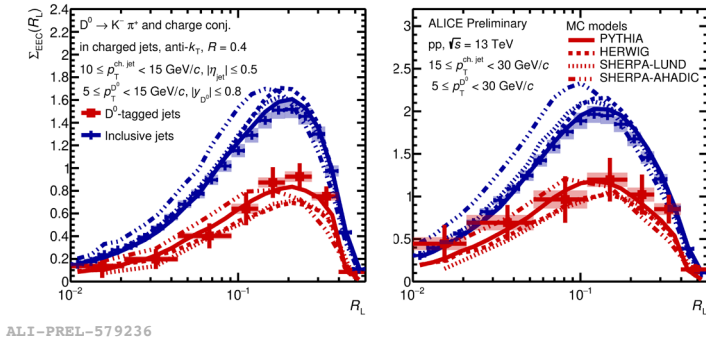


Figure 4. EECs as a function of R_L in D^0 -tagged jets in data and four event generators. The left panel shows results for 10–15 GeV/c jets, and the right panels shows 15–30 GeV/c jets. The D^0 -tagged jet EEC (red) is compared to inclusive jets (blue).

jets show an apparent preference for string-breaking models. However, neither statement is supported with overwhelming confidence by the current data.

5 First measurement of EECs in inclusive jets in p–Pb collisions

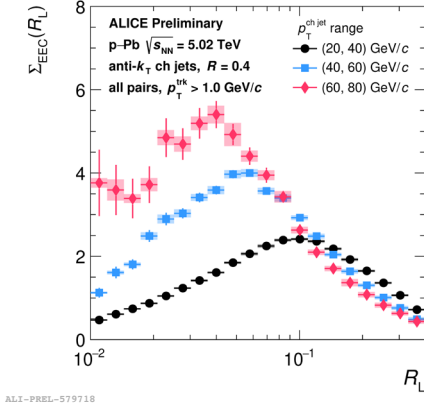
Measurements in p–Pb collisions differ from pp collisions because the parton distribution functions of the Pb nucleus differ from those of the proton, and final-state effects may also be present. Studying EECs in p–Pb collisions provides a window into interactions in small systems and cold nuclear matter.

EECs in inclusive jets in three $p_T^{\text{ch,jet}}$ ranges are considered, shown in Fig. 5. This analysis requires a background subtraction procedure with two steps. First, the $p_T^{\text{ch,jet}}$ is corrected for the underlying event (UE) following the procedure in Ref. [9]. The second step is a correction to the combinatorial background in the EEC distribution. Some of the pairs in the EEC distribution will have one or more tracks from the UE. A perpendicular cone method is used to estimate and subtract the contribution from these contaminating pairs. The same procedure is applied to the pp baseline. After corrections, the ratios of the p–Pb EEC distributions to the pp EEC are shown in Fig. 6. In the lowest $p_T^{\text{ch,jet}}$ range, a significant difference between EECs in p–Pb and pp collisions is observed. There is a distinct enhancement at large R_L , coupled with a suppression at small R_L . This modification is not visible at higher $p_T^{\text{ch,jet}}$.

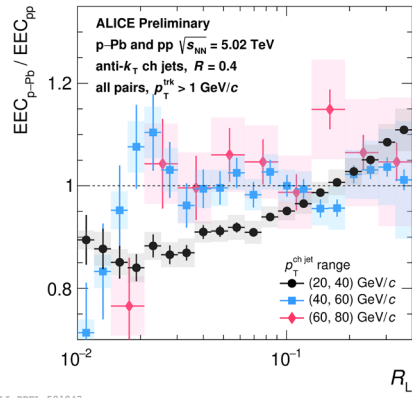
Next, the p–Pb data are inspected for the universal transition behavior found in pp. After performing the same $\langle p_T^{\text{ch,jet}} \rangle R_L$ rescalings, Fig. 5 shows that the p–Pb jets collapse onto a common shape as well. Strikingly, the peak position (2.4 GeV/c) and peak height (0.32 GeV/c⁻¹) in p–Pb are consistent with the values extracted in pp, suggesting a universality across these systems.

In all the plots presented so far, a p_T selection of 1 GeV/c is applied on the tracks from which pairs are built. Varying this cut (lowering it to 150 MeV/c and raising it to 2 GeV/c) allows its impact on the EEC to be studied. In Fig. 9, the track cut has little impact on the p–Pb/pp ratio at higher $p_T^{\text{ch,jet}}$, but changing the threshold modifies the enhancement at large R_L in 20–40 GeV/c jets while leaving the low- R_L suppression unchanged.

Finally, Fig. 9 compares the data to theoretical models. On the left is a comparison to a CGC model with varying saturation scales. This purely initial-state model fails to capture the data. In the middle are models in PYTHIA and PYTHIA Angantyr with nuclear PDFs. Standard PYTHIA shows a flat p–Pb/pp ratio. Angantyr, which models the Pb nucleus more



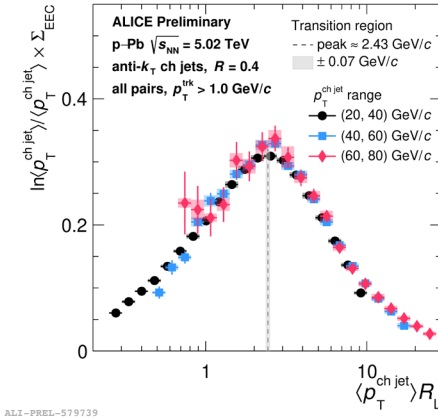
ALI-PREL-579718



ALI-PREL-581947

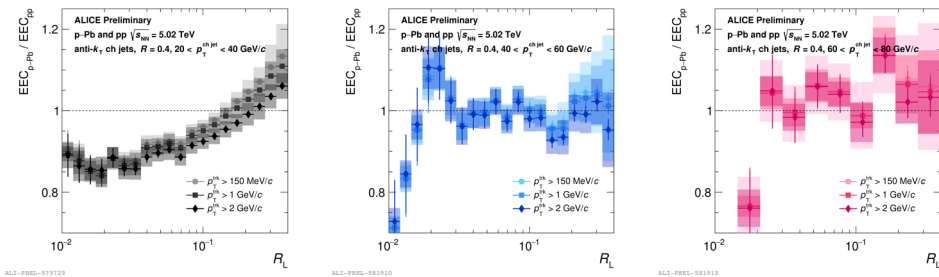
Figure 5. EECs for jets in p-Pb collisions in three $p_T^{\text{ch,jet}}$ intervals.

Figure 6. The ratio of the Σ_{EEC} distributions in p-Pb/pp collisions in three $p_T^{\text{ch,jet}}$ intervals.



ALI-PREL-579739

Figure 7. The p-Pb EECs rescaled as a function of $\langle p_T^{\text{ch,jet}} \rangle R_L$, in three $p_T^{\text{ch,jet}}$ intervals.



ALI-PREL-579729

ALI-PREL-581920

ALI-PREL-581935

Figure 8. The p-Pb/pp ratios of EECs with varying track p_T threshold.

comprehensively, replicates the suppression at small angles but fails to capture the large- R_L enhancement. The right panel presents a higher-twist calculation with varying path length L , showing that certain final-state effects can qualitatively reproduce the trends in the data. This work has been refined recently; more details can be found in Ref. [10].

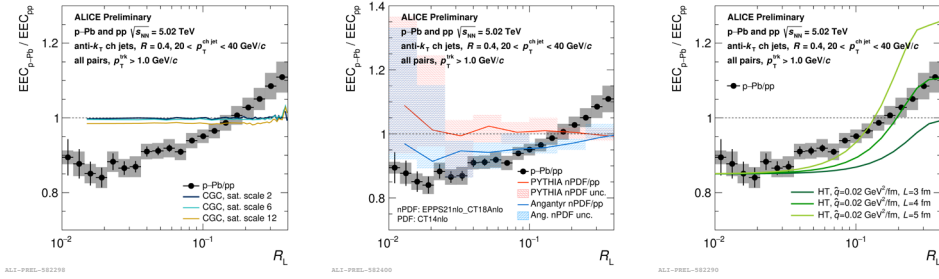


Figure 9. Comparisons of the measured EEC distributions in 20–40 GeV/c jets to various calculations and models. From left to right: a CGC model, nPDF models in PYTHIA, and a higher-twist calculation.

In summary, three new EEC measurements from ALICE are presented. The inclusive pp measurement revealed a universal EEC shape. The heavy-flavor measurement showed evidence of mass and flavor effects modifying charm jet EECs. The p–Pb measurement shows a modification relative to pp that cannot be explained by current initial-state models.

Acknowledgments

We gratefully acknowledge Haoyu Liu, Ian Moult, and Xiaohui Liu for providing CGC model predictions.

References

- [1] H. Chen, I. Moult, X. Zhang, H.X. Zhu, Rethinking jets with energy correlators: Tracks, resummation, and analytic continuation, *Physical Review D* **102** (2020). [10.1103/physrevd.102.054012](https://doi.org/10.1103/physrevd.102.054012)
- [2] K. Lee, B. Meçaj, I. Moult, Conformal collider physics meets LHC data, *Physical Review D* **111** (2025). [10.1103/physrevd.111.1011502](https://doi.org/10.1103/physrevd.111.1011502)
- [3] P.T. Komiske, I. Moult, J. Thaler, H.X. Zhu, Analyzing N -Point Energy Correlators inside Jets with CMS Open Data, *Phys. Rev. Lett.* **130**, 051901 (2023). [10.1103/PhysRevLett.130.051901](https://doi.org/10.1103/PhysRevLett.130.051901)
- [4] ALICE Collaboration, Exposing the parton-hadron transition within jets with energy-energy correlators in pp collisions at $\sqrt{s} = 5.02$ TeV (2024), 2409.12687, <https://arxiv.org/abs/2409.12687>
- [5] E. Craft, K. Lee, B. Meçaj, I. Moult, Beautiful and Charming Energy Correlators (2022), 2210.09311, <https://arxiv.org/abs/2210.09311>
- [6] P. Skands, S. Carrazza, J. Rojo, Tuning pythia 8.1: the monash 2013 tune, *The European Physical Journal C* **74** (2014). [10.1140/epjc/s10052-014-3024-y](https://doi.org/10.1140/epjc/s10052-014-3024-y)
- [7] J. Bellm, S. Gieseke, D. Grellscheid, S. Plätzer, M. Rauch, C. Reuschle, P. Richardson, P. Schichtel, M.H. Seymour, A. Siódmok et al., Herwig 7.0/herwig++ 3.0 release note, *The European Physical Journal C* **76** (2016). [10.1140/epjc/s10052-016-4018-8](https://doi.org/10.1140/epjc/s10052-016-4018-8)
- [8] E. Bothmann, G. Singh Chahal, S. Höche, J. Krause, F. Krauss, S. Kuttimalai, S. Lieb-schner, D. Napoletano, M. Schönherr, H. Schulz et al., Event generation with sherpa 2.2, *SciPost Physics* **7** (2019). [10.21468/scipostphys.7.3.034](https://doi.org/10.21468/scipostphys.7.3.034)
- [9] ALICE Collaboration, Measurement of inclusive charged-particle jet production in pp and p–Pb collisions at $\sqrt{s_{NN}} = 5.02$ TeV, *Journal of High Energy Physics* **2024** (2024). [10.1007/jhep05\(2024\)041](https://doi.org/10.1007/jhep05(2024)041)
- [10] Y. Fu, B. Müller, C. Sirimanna, Modification of the jet energy-energy correlator in cold nuclear matter (2024), 2411.04866, <https://arxiv.org/abs/2411.04866>